doi: 10.5028/jatm.v10.752 ORIGINAL PAPER

Dynamics of a Small Unmanned Aircraft Parachute System

Ashim Panta[1], Simon Watkins[1], Reece Clothier[2]

Panta A https://orcid.org/0000-0002-5452-1456
Watkins S https://orcid.org/0000-0001-5550-4941
Clothier R https://orcid.org/0000-0002-5264-3222

How to cite

Panta A; Watkins S; Clothier R (2018) Dynamics of a Small Unmanned Aircraft Parachute System. J Aerosp Tecnol Manag, 10: e1218. doi: 10.5028/jatm.v10.752.

ABSTRACT: Parachute Systems (PS) can be readily used by small Unmanned Aircraft Systems (UAS) for risk mitigation and aircraft recovery. To date there has been limited research into the fundamental dynamics of parachutes at low Reynolds numbers, with existing studies focusing on larger parachutes. An understanding of the dynamics is needed to establish sound guidelines for parachute design and for their use during UAS operations. Existing design guidelines are reviewed and the key parachute design parameters are identified. The validity of the existing guidelines applied to lower Reynolds number parachutes is explored through a series of wind-tunnel tests. It was found that existing design guidelines underpredict the key parameters of inflation time and peak forces for parachute deployments at typical UAS operating speeds. The ramifications on the design and operation of small UAS are discussed.

KEYWORDS: Parachute system, UAS, Dynamics.

INTRODUCTION

For UAS, the primary safety related hazards are: 1) a collision between an Unmanned Aircraft (UA) and other airspace users; and 2) the controlled or uncontrolled impact of the UA with terrain or objects on the terrain (*e.g.*, people or structures) (Clothier *et al.* 2015). Hayhurst *et al.* (2006) further classify these hazards into the domains of design, flight crew and operation. As discussed in Clothier *et al.* (2015), parachute systems are one of a number of devices and procedures that can be employed by UAS operators to reduce the risk to people overflown, and secondarily, to the UA and its payload.

Small commercial UAS currently exhibit a high unreliability due, in part, to the use of commercial off-the-shelf components, the limited redundancy in flight critical systems, and the uncontrollability of the UA given a failure. The high cost of payloads and the increasing use of UA in populous areas have motivated many commercial UAS operators to use parachutes.

Historically, parachute design has utilised design guidelines based on empirical data. A principle resource is Knacke's Parachute recovery systems design manual (Knacke 1992). The design guidelines established in Knacke's design manual, hereafter referred to as Knacke's guidelines, are derived from experimental testing of large parachutes at Reynolds numbers (Re) on the order of 10^7. Knacke established the boundary and performance ranges of parachute operations, which have been applied to parachute envelopes greater than 20 foot in diameter deployed at speeds greater than Mach 0.2 and from altitudes of 5,000 ft or higher. The vast majority of small UA (*e.g.*, of maximum takeoff mass less than two kg) currently operate at much lower Re (in the order of 10^5) and at altitudes below 400 ft above ground level (this operational height limit is due to regulatory constraints as opposed to the operational capability of the UA).

1.RMIT University – School of Engineering – Aerospace Engineering and Aviation – Melbourne/VIC – Australia. **2.**Brisbane Technology Centre – Boeing Research & Technology – Melbourne/VIC – Australia

Correspondence author: Ashim Panta | RMIT University – School of Aerospace Engineering and Aviation | Plenty Road - Bundoora 3083 – Melbourne/VIC – Australia | Email: ashim.panta@rmit.edu.au

Received: Nov. 29, 2016 | **Accepted:** Feb. 05, 2017

Section Editor: Valder Steffen Jr.

Despite these differences, Knacke's guidelines have been applied in the design of parachute systems (PS) for UAS (Cartwright 2008; Butler and Montanez 2007; Wyllie 2001), with minimal consideration as to the validity of their use. Butler and Montanez (2007) address common issues associated with the design, testing and qualification of PS for a range of UAS scales. Based on Knacke's guidelines, the authors illustrate the way key physical parameters of a parachute are sized for UA platforms with a clear layout of the design procedure. Cartwright (2008) again applies Knacke's guidelines to design a PS for a 25 kg UA. Cartwright investigates the possibility of inflating a small parachute without losing altitude. The study used data from a series of parachute deployments from a moving motor vehicle. The inflation times were recorded to derive the altitude loss during deployment of the canopy. These existing studies make use of existing parachute design guidelines with minimal consideration as to the validity of their use.

This paper explores the validity of existing parachute guidelines, and in particular those described in Knacke (1992), for small UA. The existing design guidelines for key parachute design parameters are presented. The validity of the existing design guidelines are explored through a comparison of results obtained from wind-tunnel experimentation. The experimental setup is also presented. The experiments utilised a representative parachute, which is applicable to UA of maximum takeoff mass of up to 2 kg. This mass restriction was chosen as:

- It is representative of many common commercial fixed and multi-rotor UA types (Fig. 1);
- The applicable parachutes are of a size that can be readily tested within available wind-tunnel facilities; and
- Parachutes applicable to UA of this size can be readily bought off-the-shelf. Testing was undertaken for the three operational speeds of 48, 68, and 105 km/h. These speeds are representative of the average stall, cruise, and maximum speeds (respectively) determined for a wide range of fixed wing UA (Fig. 2). The results from wind-tunnel experiments are presented later in this paper.

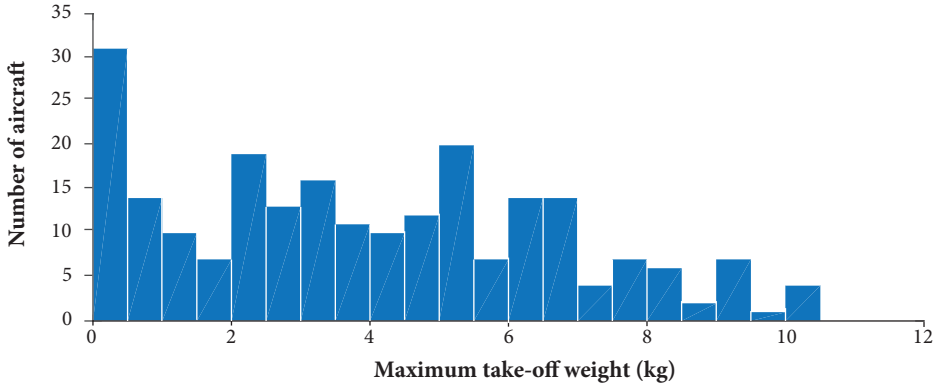

Figure 1. Distribution of maximum takeoff weights of sub-10 kg fixed wing unmanned aircraft (Palmer and Clothier 2013).

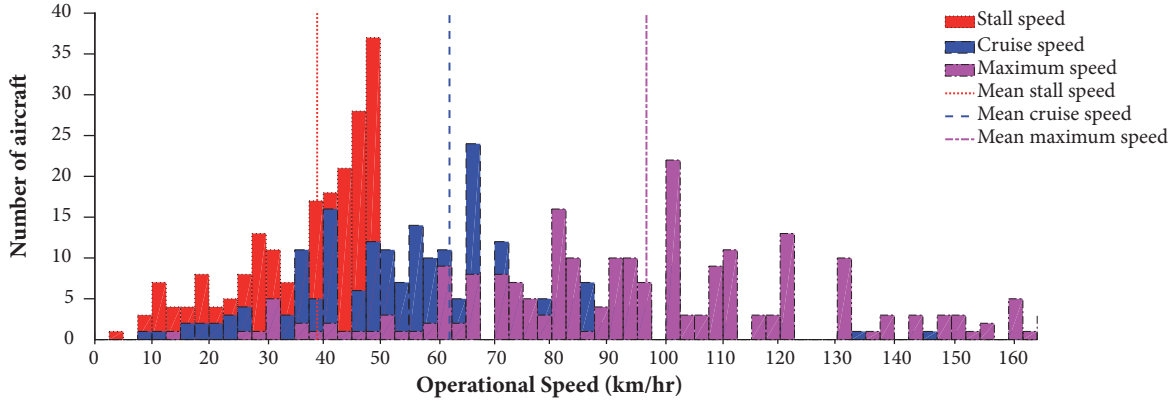

Figure 2. Market assessment of typical operating speeds of sub-10 kg fixed wing unmanned aircraft (Palmer and Clothier 2013).

EXISTING PRINCIPLES

ANATOMY OF A PARACHUTE

Detailed anatomy of PS is described in Knacke (1992). A typical simple PS assembly is shown in Fig. 3. The payload, in this instance, is the UA, which is attached via the riser line to the main chute via a series of shroud lines. The main chute (also referred to as the main canopy) provides the principle source of drag and is typically made out of a lightweight material resistant to tearing and with low porosity (*e.g.*, nylon).

The gore refers to the section of the parachute canopy between two load bearing members running from the suspension lines at the skirt to the top of the canopy. The riser line is typically made out of spectra or Kevlar™, the elasticity of which helps to reduce the shock imparted on the airframe during the chute deployment.

Attached to the top of the main chute via the bridle is the pilot chute. The function of the pilot chute is to pull out the main canopy from a deployment bag. The pilot chute and deployment bag provide additional drag, however, the relative drag contribution is fairly small compared to that of the main canopy during steady state/descent conditions.

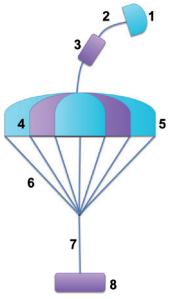

1. Pilot chute
2. Bridle
3. Deployment bag
4. Gore
5. Main canopy
6. Shroud lines
7. Riser
8. Payload

Figure 3. Anatomy of a parachute assembly.

THE INFLATION PROCESS

The typical parachute inflation process is described in Knacke (1992) and summarised here. The force-time profile is illustrated in Fig. 4. The parachute inflation process starts at T_0 with the pilot chute being extracted from a deployment container. The force exerted from the inflation of the pilot chute at T_1 initiates the deployment of the main canopy. The shroud lines get drawn as the canopy inflates due to the airflow accumulating within (between T_1 and T_2). The main canopy continues to inflate until the payload reaches a steady-state descent velocity.

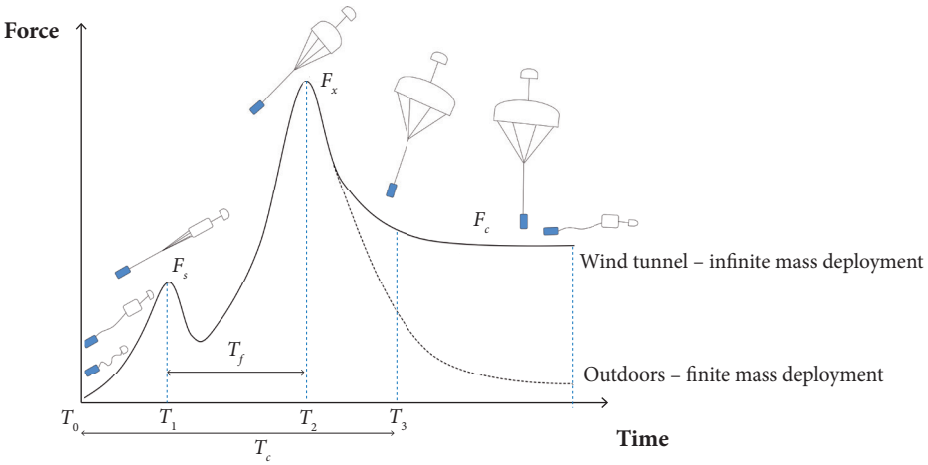

Figure 4. Force-time profile of a parachute across its deployment stages, adapted from Knacke (1992).

Deployment characteristics of a parachute will differ depending on whether the payload is fixed to an infinite mass (such as a force balance secured in a wind tunnel) or whether the payload is free to move (finite mass test such as a deployment from a flying UA). As discussed by Knacke (1992), infinite mass tests result in a higher steady-state force as seen in Fig. 4.

SIGNIFICANT PARACHUTE DESIGN PARAMETERS

A principal resource in the design of PS, Knacke (1992) establishes the rules of thumb for calculating the various design parameters illustrated in Fig. 4. The design guidelines are largely based on empirical data obtained from experimentation of chutes operating in Re greater than 10^7. The key parachute design parameters, illustrated in Fig. 4, are the pilot chute force (F_s), the main canopy force (F_x), steady-state descent force (F_c), chute inflation time (T_f), and the time it takes to reach steady-state descent (T_c).

The pilot chute force (F_s) determines the design load on the bridle and the force required to pull out the main canopy from its deployment bag. F_s can be estimated using Eq. 1, *i.e.*, treating the pilot chute as a canopy on its own. F_x dictates the maximum load exerted on the riser and the point of attachment onto the aircraft. Structural design of the link between the PS and the UA is largely determined by F_x and hence it is a key design consideration for both the PS and the UA. As there is a direct correlation between surface area and speed, F_x depends on canopy shape, size, and airspeed. Based on the force-velocity trajectory method described in Mickey *et al.* (1970) and McEwan (1970), F_x is determined from the relationship given in Eq. 1, from Knacke (1992).

$$F_x = (C_d S)_{parachute} q C_x X_1 \tag{1}$$

where $(CdS)parachute$ is the drag area of the fully open parachute in ft^2, q is the dynamic pressure at canopy stretch, in lb/ft^2, C_x is the opening force coefficient. C_x indicates the differences between instantaneous opening force and steady drag force at a constant speed (1.6 from Knacke 1992). X_1 is the opening force reduction factor. Theoretically, in an infinite mass condition, the force reduction factor is 0.9 for the main canopy.

The steady-state force (F_c) determines the steady-state descent rate of the UA, which is an important factor in determining the time required to slow the UA down, and in turn the minimum height from which a deployment can be made. As will be shown later, the steady-state forces exerted during the wind-tunnel tests were oscillating in an approximately sinusoidal manner. Hence, an average of those fluctuating forces was assumed to be the steady state-force in this research. Traditionally the steady-state force is said to be the ratio of the peak force due to the inflation of the main canopy to the opening force coefficient (Knacke 1992), as given in Eq. 2.

$$F_c = \frac{F_x}{C_x} \tag{2}$$

Inflation time (T_f) is the duration of time between the full inflation of the pilot chute and the main canopy, as shown in Fig. 4. T_f dictates the time required to pull the main canopy out of the deployment bag. Based on results from free flight tests, T_f for a solid flat circular parachute is determined by Knacke (1992), as shown in Eq. 3.

$$T_f = \frac{nD_o}{v0.85} \tag{3}$$

where D_o, nominal parachute diameter *ft* ; v is velocity in *ft/s*, n is filling constant indicating the filling distance as a multiple of D_o. For canopies with a standard porosity, Knacke states to use $n = 4.0$.

Time to reach steady-state descent (T_c) indicates when the parachute reaches steady-state descent. The existing literature does not provide a consistent definition for determining T_c from the force-time plot.

Froude number (F_r) has a significant influence on the opening force and inflation time (Cockrell and Young 1987, Lee 1989):

$$F_r = \frac{v^2}{gD_o} \propto \frac{1}{R_m C_D} \tag{4}$$

where g is gravity and R_m is the measure of the ratio of air mass enclosed in the fully inflated parachute canopy to the payload mass. For a given drag coefficient the F_r is inversely proportional to R_m. The effects of F_r are significant when small F_r and large R_m are combined, *e.g.* when heavily loaded parachutes are deployed at low speeds (Wolf 1974). Conventional parachute designs are characterized by low F_r and R_m (Cockrell and Young 1987). Johari and Desabrais (2003) stated that F_r does not play a significant role in an infinite airflow conditions. Hence, the effects of F_r are not addressed in this project as the testing was done in a wind tunnel to a lightly loaded parachute.

WIND-TUNNEL TESTING

To explore the validity of these design guidelines at Re applicable to small UAS, a series of wind-tunnel tests were undertaken. Experimentation involved measuring the force-time profile for a single representative parachute for repeated deployments within a wind tunnel.

REPRESENTATIVE PARACHUTE

A single representative parachute was chosen for experimentation. The characteristics of the chute for a sub-2 kg UA and impact speed of between 5 – 8 m/s were determined using the design guidelines presented by Knacke (1992). Designing for this descent velocity ensured that the cross section of the parachute was < 6% of the wind-tunnel test cross section. Historically without any blockage correction, the test data is considered acceptable with the blockage ratio < 6%.

A round canopy shape with hemispherical back was selected as it provided the simplest case for analysis and provides a greater C_d amongst a range of parachute types presented by Knacke (1992). A survey of 21 UAS with a maximum takeoff mass of under 150 kg revealed that, over 75% of the PS consisted of round canopy type. A review was then undertaken of commercially available parachutes. The parachute with parameters closest to those calculated using Knacke's guidelines was selected and used as the characteristic chute for experimentation. The characteristic chute chosen had a diameter of 24 inches. Table 1 summarises the parameters used to select the chute and the final parameters of the chute chosen for experimentation.

Table 1. Parameters used for parachute selection and final parameters of the parachute chosen for experimentation, based on total weight, W_t (mass = 1.2 kg).

Design parameters	Knacke's guidelines (Knacke 1992)	Parachute
Coefficient of drag, *Cd*	0.65-0.95	1.6
Drag area, *Sparachute* (m^2)	0.54 (Eq. 5)	0.29
Canopy diameter, D (m)	0.83 (Eq. 6)	0.60
Riser length, *Sf* (m)	3.33 (Eq. 7)	2.43

$$S_{parachute} = \frac{2W_t}{C_d v^2 \rho} \tag{5}$$

$$D_o = \sqrt{\frac{S_{parachute}}{4\pi}} \tag{6}$$

$$S_f = nD_o \tag{7}$$

A sufficiently long riser length was chosen to ensure that adequate time was provided for full inflation of the main canopy and there was enough distance downstream of the deployment rig for minimal influence from the rig's wake (Fig. 5). Using the design guidelines presented in the previous section, the key design parameters were calculated for the characteristic parachute and are summarised in Table 2.

Table 2. Key canopy parameters evaluated from Knacke (1992) during the design of the characteristic parachute.

Parameters	Stall speed	Cruise speed	Maximum speed
Peak force, F_x (N)	136	270	622
Steady-state force, F_c (N)	85	169	388
Inflation time, T_f (s)	0.146	0.104	0.069

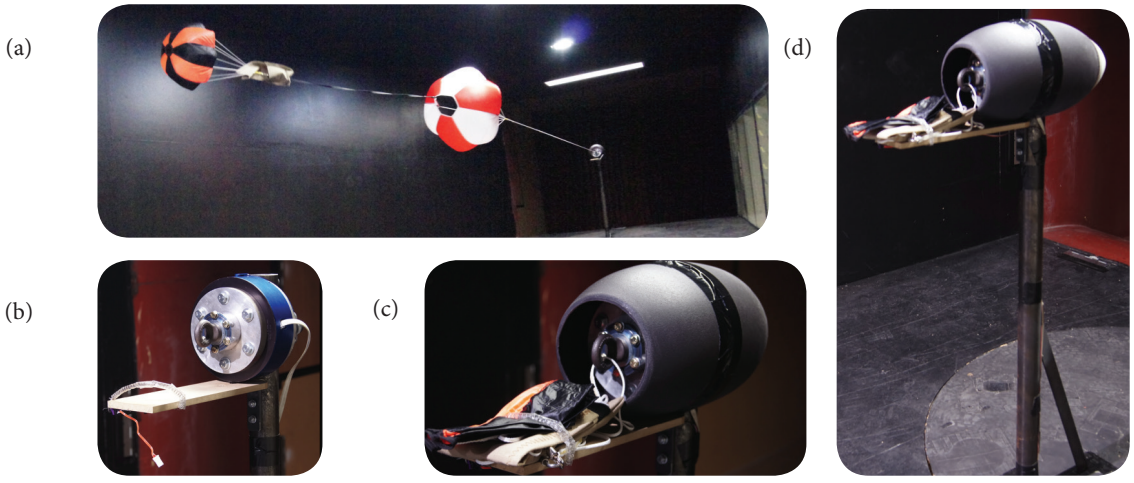

Figure 5. PS system during a fully inflated stage in the wind-tunnel (a), force balance sensor (b), spring-based deployment mechanism (c) and deployment rig (d).

DEPLOYMENT RIG

A deployment rig featuring a mechanical release mechanism was designed to consistently launch the parachute down the centre of the tunnel. The rig was made using a cylindrical pole with a platform at one end to accommodate a force balance as shown in Fig. 5. A streamlined nacelle was used to minimise the wake and turbulence region downstream of the deployment rig.

INSTRUMENTATION

A dynamic force balance was used to measure the force-time profile during deployment of the parachute. The force balance, manufactured by JR3 Multi Axis Load Cell Technologies, can measure force along three orthogonal axes (x, y and z) to a stated nominal accuracy of ± 0.25%. the output measurements from the digital balance were read at a maximum frequency of 1000 Hz via a digital signal connection.

Dynamic pressure readings from the pitot tube located inside the tunnel were used to evaluate the airspeed using Eq. 8.

$$v = \sqrt{\frac{2P_{atm}}{\rho}} \tag{8}$$

where v is velocity in m/s, P_{atm} is atmospheric pressure in P_a, ρ is air density, P_{atm}/RT in kg/m^3. R is universal gas constant, 287.058 in J/kgK, T is temperature inside the tunnel in K.

CALIBRATION

A Turbulent Flow Instrumentation Cobra Probe™ (Turbulent Flow Instrumentation 2015) was used to calibrate the wind tunnel between air speeds from 40 km/h to 110 km/h. The Cobra Probe was used to measure the turbulence intensity at various points upstream and downstream of the deployment rig, as shown in Fig. 6. This was done to determine the turbulent flow intensity and the velocity deficit of the flow upstream and downstream of the tunnel. It was found that the wake turbulence generated by the rig was within 1.5% of the free stream turbulence of the tunnel at the location of full canopy inflation. Attained results closely matched those presented in previous studies to calibrate the wind-tunnel test environment (Ravi 2011).

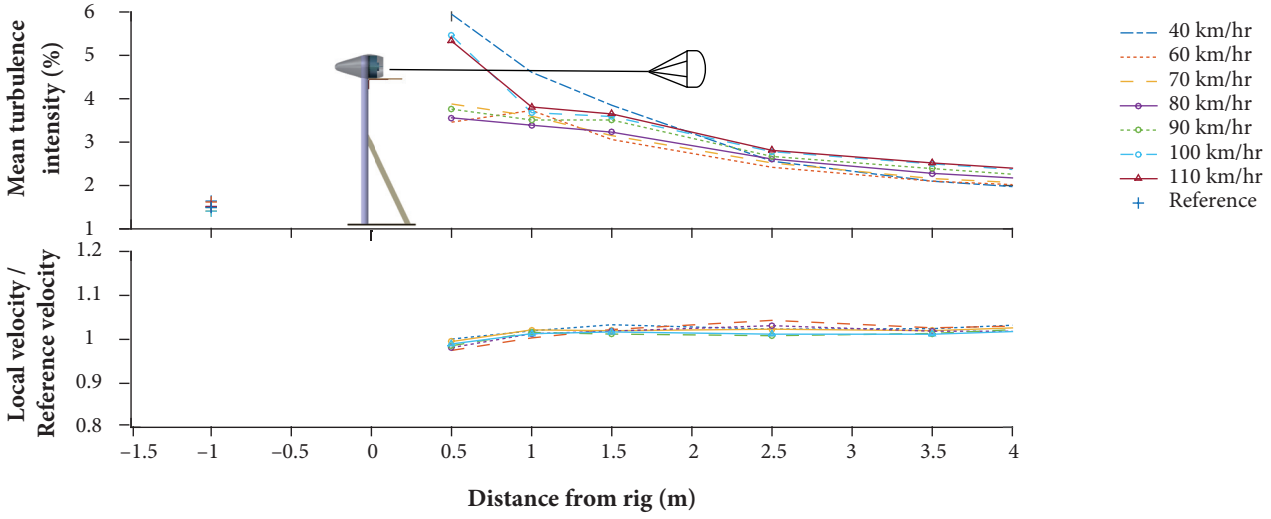

Figure 6. Wind-tunnel calibration data using a Cobra Probe™.

A simple static calibration test was conducted on the load cell to check its accuracy and it was found to be linear and accurate to ± 1%. A dynamic response test was undertaken to determine whether the response of the force balance was interfering with the force data being logged. This involved manually tapping the load cell and recording the response.

RESULTS

The force exerted during the deployment of the PS was recorded in real time. This was done using data logging software running on a computer connected to the JR3 digital force balance. Twenty deployments were recorded at each of the three deployment airspeeds of 48, 68, and 105 km/h. Through visual observation it was ensured that deployments where the parachute did not inflate properly, or when the parachute left the working cross-section of the tunnel (*i.e.*, came close to the tunnel walls or floor) were excluded from the results. For each run, four seconds of datawere recorded, as the parachute would generally finish the inflation process within the first second. These data were then imported to Matlab™ for processing and analysis.

Box plots are used to represent the range of forces and inflation time achieved from the experiments. Figure 7 shows the definition of the box plots elements. The central line marks the data set median. The height of the box represents the interquartile range (IQR) of the data set. The ends of the whiskers (lines extending from the boxes) mark the highest and lowest values of the data set. The plus signs mark individual values outside the range of the whiskers, the bottom of the box marks the 25th percentile for the data set. The approximate definition of 25th percentile is the value such that 25% of the data set values are below and 75% of the data set values are above. The top of the box marks the 75th percentile for the data set.

Forces exerted during deployments were logged with respect to real time. All average results presented in the report are processed with smooth spline curve fitting in Matlab in order to get average data. An analysis of the goodness of fit is provided later.

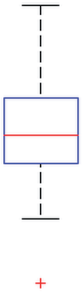

Figure 7. Anatomy of a box plot.

FORCE AND TIME PROFILES MEASURED FROM THE WIND-TUNNEL TESTS

The force-time plots for the three different deployment speeds are given in Figs. 8-10. As can be observed, there is significant variation in the measured results despite consistent deployment launch conditions. The oscillations seen in Figs. 8-10 could possibly be attributed to the presence of vortex shedding around the parachute. The dominant oscillation frequencies using a Strouhal

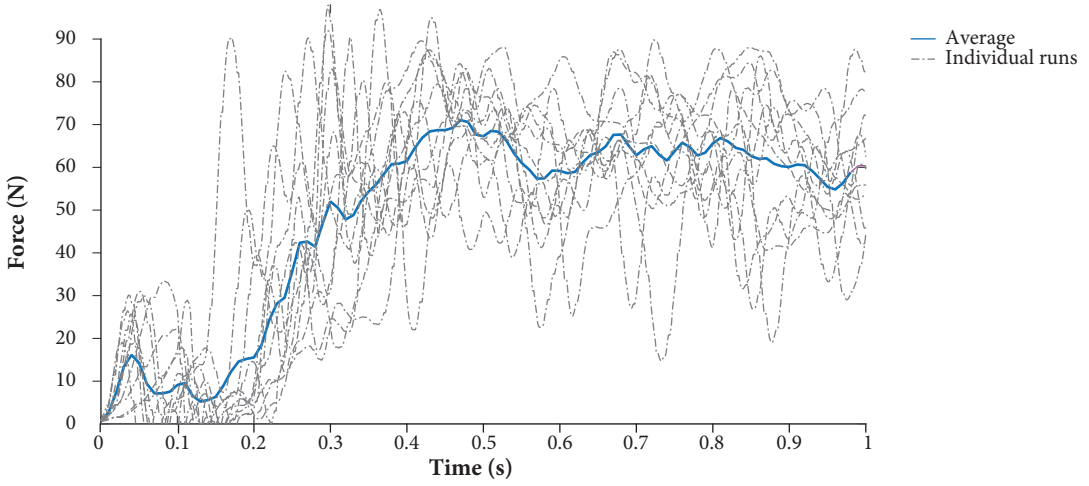

Figure 8. Force and time profiles at 48 km/h (stall speed).

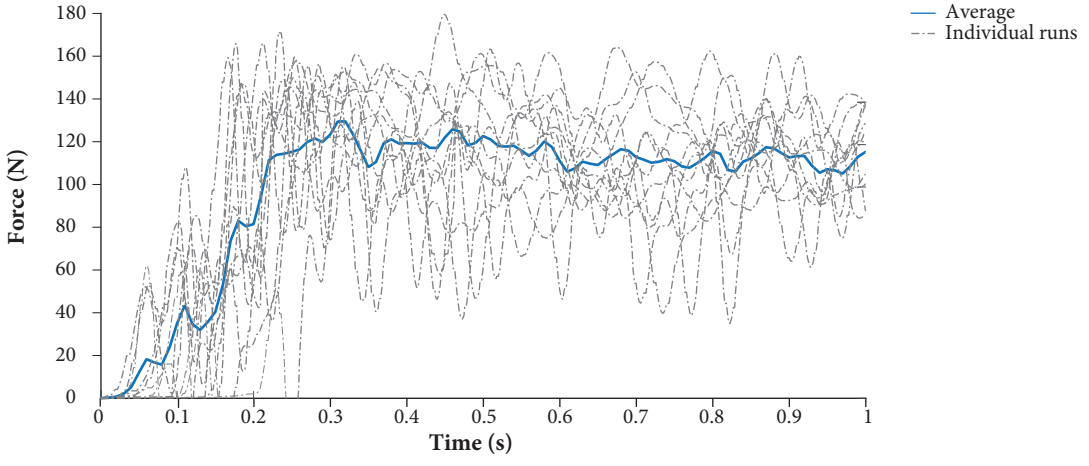

Figure 9. Force and time profiles at 68 km/h (cruise speed).

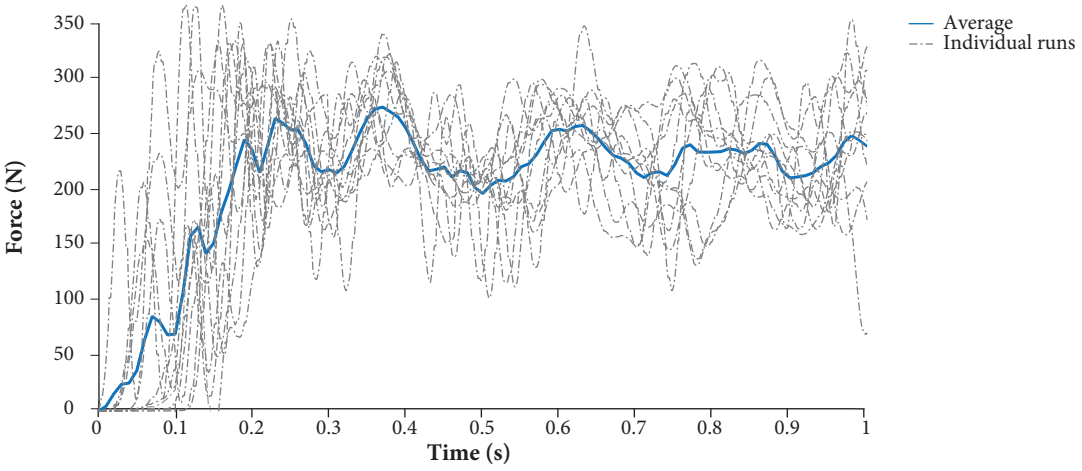

Figure 10. Force and time profiles at 105 km/h (maximum speed).

number of 0.2 were found to be 4, 6 and 10 Hz for stall, cruise, and maximum deployment airspeeds, respectively. An inspection of the typical frequencies of force oscillations from Figs. 6-8 as well as a spectral analysis of the time series data showed that these are the dominant frequencies in the force-time graphs. The results achieved from wind-tunnel experimentation demonstrated that the dynamic testing of a parachute is complex in nature.

As to be expected, it was found that the peak forces were exerted when the main canopy fully inflates for the first time, as displayed in Figs. 8-10. The mean magnitude of the forces determined from wind-tunnel testing were 20%, 9% and 1% greater than what were calculated using Eq. 1 for deployments at stall, cruise, and maximum airspeeds, respectively. The comparison of results suggest that Knacke's guidelines provide a more accurate prediction of the forces with increasing speed. This is somewhat expected, as the test Re approach the typical Re used to determine the design guidelines.

Whilst designing small parachutes, it is essential to keep in mind that F_x of the designed parachute will actually be greater than what Knacke's guidelines evaluates. As F_x affects the load exerted on the point where the PS is connected to the UA, the structural design of the joint and riser needs to be overdesigned.

PEAK FORCE F_x

A comparison of the measured and calculated peak (F_x) and steady-state forces (F_c) are provided in Fig. 11. As expected, the magnitude of F_x and F_c increases with airspeed.

FORCE DURING STEADY-STATE DESCENT F_c

Figure 11 shows that F_c exerted during the wind-tunnel tests is also underpredicted by Knacke's guidelines. Similar to the peak force, it was found that the difference between experimental and predicted results decreases with increasing speed. Measurements of F_c from the tunnel testing revealed values 33%, 26%, and 8% greater than the F_c predicted using Knacke's guidelines for stall, cruise, and maximum deployment airspeeds, respectively. This finding implies that the UA might impact the terrain at lower velocity than initially expected. Hence using Knacke's guidelines for estimating F_c will in-fact provide the design with a safety margin, as in reality the UA under the parachute will have a greater drag force, and ultimately a lower impact velocity, during descent.

INFLATION TIME T_f

Knacke's guidelines further underpredicted the mean T_f by up to 153% and 24% for stall and cruise speed, respectively (Fig. 12). The measured mean T_f at maximum deployment airspeed is within 1% of that calculated using Knacke's guidelines. The T_f calculated using Eq. 3 assumes that the parachute canopy has standard porosity and is a solid flat circular canopy. As the main

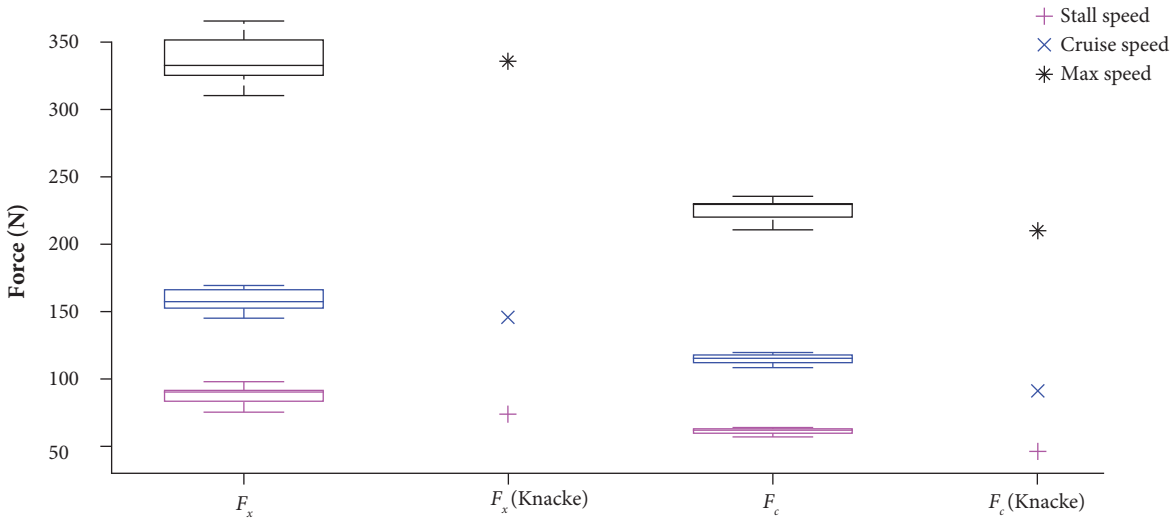

Figure 11. Comparison of peak force and steady-state force exerted during the wind-tunnel tests against the predicted values from Knacke's guidelines for an infinite mass condition.

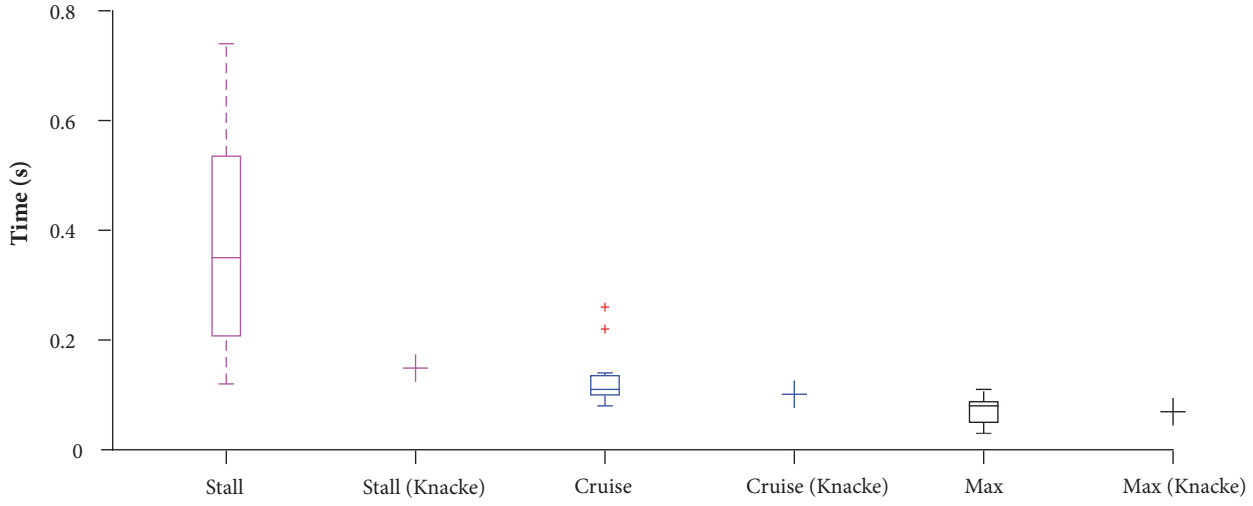

Figure 12. Comparison of inflation time during the wind-tunnel tests against the predicted values from Knacke's guidelines for an infinite mass condition.

canopy tested in the wind tunnel is hemispherical, the differences in their aerodynamic properties is not considered by Eq. 3. Measured results indicate that the main chute will take longer to fully deploy than would be determined using existing guidelines, particularly for lower speeds. This finding would be most critical for those UA operations at low altitude and low speeds (*e.g.*, UA immediately on climb or descent) approach.

TIME TO REACH STEADY-STATE DESCENT T_C

Existing literature did not provide a precise means for estimating T_c. In this paper, it is assumed to have reached steady state when the force and time profile surpasses the average oscillation force for the second time following F_x (Fig. 13). The average force was derived from random sampling of the tail end of the force and time profile.

As can be observed from Fig. 14, T_c tends to increase at higher airspeeds, with the parachute expected to reach its steady state descent the quickest at the highest deployment airspeed.

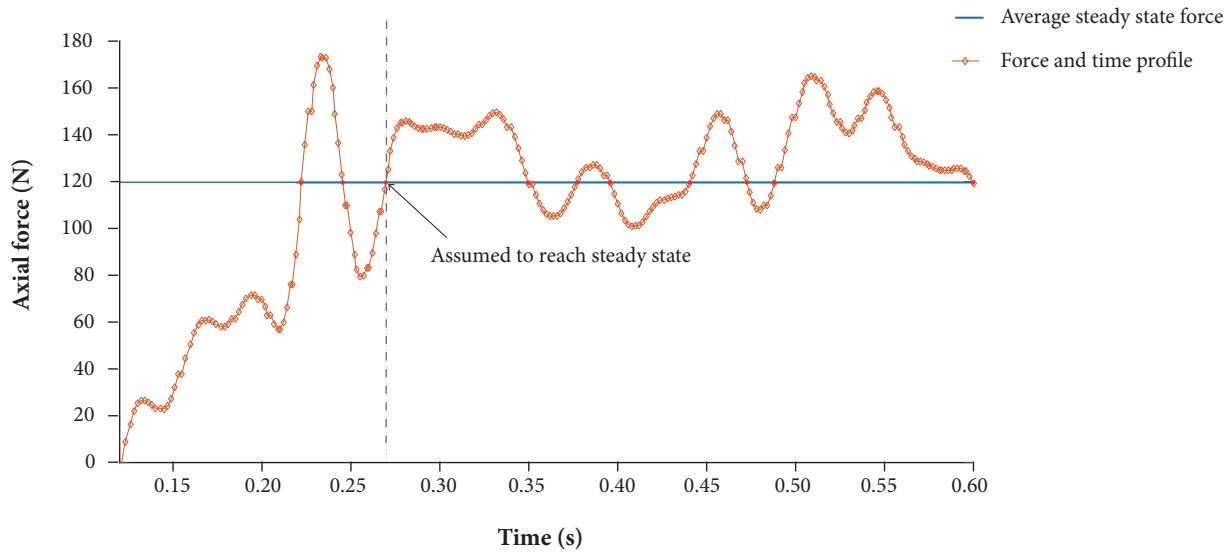

Figure 13. Evaluation of time to reach steady state adopted for this research.

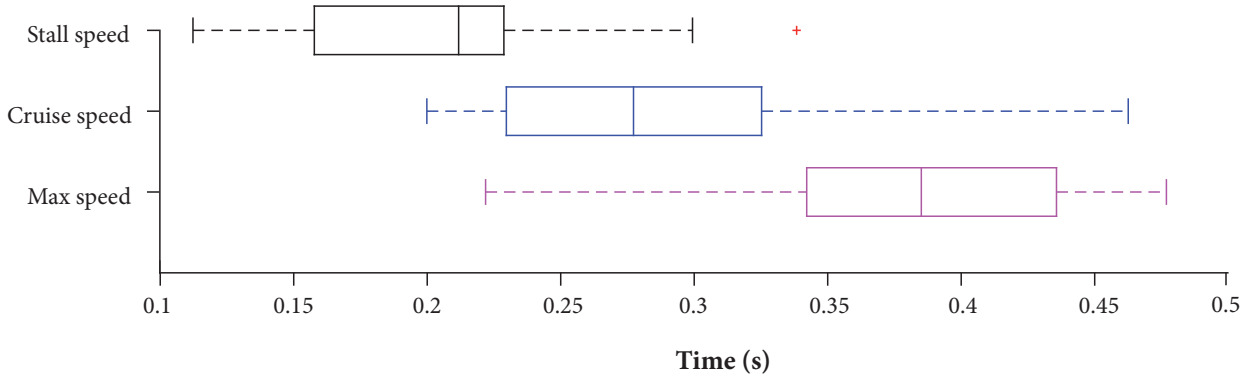

Figure 14. Time to reach steady-state descent at typical UAS operating speeds.

A parachute deployed at maximum airspeed reaches steady state almost twice as fast as one deployed at stall speed. The T_c correlates directly to airspeed, hence at greater speed the pilot chute fills up faster, causing the main canopy to inflate faster and reach steady-state descent quicker.

PILOT CHUTE FORCE F_s

Results from the wind-tunnel tests show that between the stall and maximum deployment airspeeds, forces exerted from the inflation of the pilot chute are 25% to 102% greater than the estimations determined through the use of Knacke's guidelines. Review of the deployment video footage revealed partial pull out of the main canopy from the deployment container prior to the complete inflation of the pilot chute. At greater airspeeds, it was found that the main canopy was being pulled out of its deployment bag before the pilot chute achieved complete inflation. This contributes to the increase in force and difference between results determined from experiments and estimations from Knacke's guidelines, as experimentally measured F_s consists of the forces exerted by the partial deployment of the main canopy in addition to the force exerted from the full inflation of the pilot chute. Knacke's guidelines also do not consider the dynamics from the spring constant of the riser lines and the shroud lines.

CORRECTION FACTOR *P*

As observed, the key governing equations to predict the peak force, Eq. 1, steady-state descent force, Eq. 2, and finally the inflation time, Eq. 3, all underestimated the respective parameters. The differences were dependent on the airspeed. Thus, Fig. 15 is developed to provide the correction factor as a function of airspeed so that governing equations from Knacke produced results of better match to experiment. For Eqs. 1-3, the correction factor, *P*, is to be applied as a divisor. *P* is simply the ratio of the difference between theoretical and experimental results. It is inappropriate to conclude that the correction factor scales for other chute designs, sizes and speeds beyond the scope of the experimental matrix presented in this research.

An hypothesis statistical t-test assuming unequal variances suggested that specially for lower speeds (stall and cruise speeds representative), Eqs. 1-3 provided a poor estimation of the respective parameters. For the fastest airspeed case, the test encouraged the use of Knacke's principle equations. Thus, it is highly possible that the differences could be due to the effects of Reynolds number.

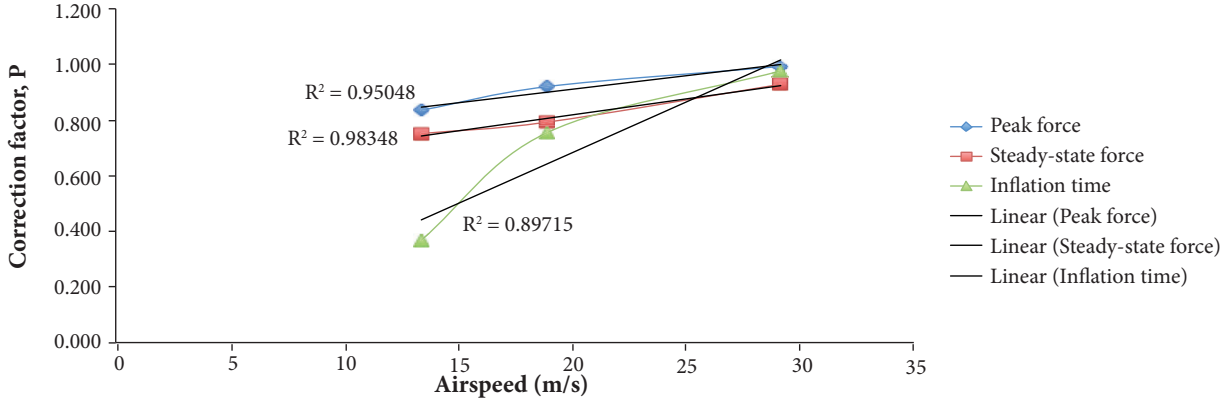

Figure 15. Correction factors for forces and inflation time for typical UAS operating speeds.

GENERAL ERROR CONSIDERATIONS

Throughout the wind-tunnel testing, the parachute was assumed to be perfectly deployed down the centre of the tunnel. Thus, the forces exerted by the parachute only account for the force exerted down the centre of the tunnel. Through analysis of the recorded visual footage and of the forces recorded by the 6-DOF force balance, it was found that a maximum of 5% of the peak force were being exerted on the lateral and vertical axis during the deployment stages.

The repeatability of the recorded force profile is dependent on the consistency of the packing of the parachute and coiling of the riser line. To reduce the potential variability in results, the parachute was always folded in accordance to the manufacturer's instructions. The data presented in Figs. 6-8 were sampled such that the inflation process started at t=0. Slight variation in the process of packaging the chute would have caused significant variation at where the peak force occurred. Thus, the average forces recorded do not consider the lag in time on each peak force.

The goodness of curve fitting is presented in Table 3.

Table 3. The goodness of the curve fitting (smooth spline) done during data processing in Matlab.

Goodness of curve fitting	Value
The sum of squares due to error (SSE)	277.4
R-square	0.9997
Adjusted R-square	0.9992
Root mean squares error (RMSE)	0.8983

CONCLUDING REMARKS

The aim of this research was to improve knowledge in the design of parachutes for low Reynolds number UAS operations. The objective was to explore the validity of generally accepted design guidelines through a comparison with experimental results obtained from wind-tunnel testing.

The comparison of mean forces and time from the experiments revealed a number of differences, which can have significant impact on the design and operation of small UAS. The comparison shows that the general guidelines underpredict the peak forces exerted by the main canopy, the steady-state descent force, and the mean time to inflation. Underestimation of the peak force during the inflation of the main canopy can increase the risk of structural failure at the mounting point to the UA, or failure in the riser lines. However, the magnitude of the underestimation is largest at lower airspeeds. Likewise, the existing guidelines tend to underestimate the inflation time, suggesting that the minimum deployment height would need to be higher than that determined through using the existing guidelines. The underestimation of the steady-state force is advantageous to designers, as the parachute, in reality, is likely to have a higher drag, decelerating quicker, and having a lower impact velocity than predicted through existing design guidelines.

In conclusion, the design guidelines from Knacke, which have been widely used to design PS for the UAS industry, underpredicts the forces exerted during deployment, steady-state descent and inflation time. The underprediction of the peak force calls for an additional consideration in designing the connection between the parachute and the UA, whereas the underprediction of the steady-state force provides an additional margin of safety.

This work was undertaken for a single representative parachute. It is recommended that further experimentation be undertaken to account for other parachute designs commonly used by UAS. Comparisons should also be made against those evaluated using an alternate design guidelines presented in Pflanz (1942) and to computerised force-time trajectory methods. The force and time data generated from the wind-tunnel testing will be used to develop a dynamic model of a sub-2 kg fixed wing UA subject to parachute deployment following a system failure, including landing conditions. The dynamic model will focus on investigating the influence of initial deployment conditions, operational envelopes, and wind on UA impact location and speed. Likewise, to improve the physical meaning of the average peak forces, it is recommended to hold the peaks of the forces at the same moment in time.

AUTHOR'S CONTRIBUTION

Conceptualization, Clothier R and Watkins S; Methodology, Panta A, Watkins S and Clothier R; Investigation, Panta A, Watkins S and Clothier R Writing – Original Draft, Panta A; Writing – Review & Editing, Panta A, and Watkins S; Funding Acquisition, Panta A and Watkins S; Resources, Panta A and Watkins S; Supervision, Clothier R and Watkins S.

REFERENCES

Butler MC, Montanez R (2007) The selection and qualification of a parachute recovery system for your UAV. SAE Technical Paper number 2007-01-3928. doi: 10.4271/2007-01-3928

Cartwright KGS (2008) Feasibility of parachute recovery systems for small UAVs. The UNSW Canberra at ADFA Journal of Undergraduate Engineering Research 1(1).

Clothier R, Williams B, Washington A (2015) Development of a template safety case for unmanned aircraft operations over populous areas. SAE 2015 AeroTech Congress and Exhibition, Seattle. doi: 10.4271/2015-01-2469

Cockrell DJ, Young AD (1987) The aerodynamics of parachutes. Neuilly-sur-Seine: AGARD.

Hayhurst KJ, Maddalon JM, Miner PS, DeWalt MP, McCormick GF (2006) Unmanned aircraft hazards and their implications for regulation. 25th Digital Avionics Systems Conference, 2006 IEEE/AIAA, IEEE, p. 1-12. doi: 10.1109/dasc.2006.313735

Johari H, Desabrais K (2003) Stiffness scaling for solid-cloth parachutes. Journal of Aircraft 40(4):631-638. doi: 10.2514/2.3166

Knacke TW (1992) Parachute recovery systems: design manual. Santa Barbara, CA: Para Publishing.

Lee CK (1989) Modeling of parachute opening – an experimental investigation. Journal of Aircraft 26(5):444-451. doi: 10.2514/3.45783

McEwan A (1970) An investigation of parachute opening loads, and a new engineering method for their determination. 3rd Aerodynamic Deceleration Systems Conference; Dayton, USA. doi: 10.2514/6.1970-1168

Mickey F, McEwan A, Ewing E, Huyler W (1970) Investigation of prediction methods for the loads and stresses of Apollo type spacecraft parachutes. Volume 1: Loads. Newbury Park: Northrop Corporation.

Palmer J, Clothier R (2013) Analysis of the applicability of existing airworthiness classification schemes to the unmanned aircraft fleet. Proceedings of 15th Australian International Aerospace Congress (AIAC15-AERO); Melbourne, Australia, p. 228-244.

Pflanz E (1942) Determination of the decelerating forces during the opening of cargo parachutes. USAF Translation to German Report FGZ 231.

Ravi S (2011) The influence of turbulence on a flat plate airfoil at Reynolds numbers relevant to MAVs (PhD thesis). Melbourne: RMIT University.

Turbulent Flow Instrumentation (2015) Cobra probe references; [accessed 2017 Nov. 17]. http://www.turbulentflow.com.au/Products/CobraProbe/CobraReferences.php

Wolf D (1974) A simplified dynamic model of parachute inflation. Journal of Aircraft 11(1):28-33. doi: 10.2514/3.60317

Wyllie T (2001) Parachute recovery for UAV systems. Aircraft Engineering and Aerospace Technology 73(6):542-551. doi: 10.1108/aeat.2004.12776baf.001